



TECHNICAL ARTICLE

# Tailoring Biodegradation of Mg-Ca Alloy by Acid Pickling and Polydioxanone/n-Hydroxyapatite Composite Coating for Temporary Implant Applications

Mathew Gaius Cherian, Shebeer A. Rahim, V.P. Muhammad Rabeeh, M.A. Joseph, and T. Hanas

Submitted: 6 January 2022 / Revised: 17 March 2022 / Accepted: 25 April 2022 / Published online: 12 May 2022

Magnesium (Mg) based alloys are good candidates for developing degradable metallic implants. Mg can easily degrade in a physiological environment without producing any toxic by-products. However, the degradation rate needs to be controlled to make it compatible with the tissue growth rate. Achieving enhanced degradation resistance and biological performance in the physiological environment without sacrificing its mechanical and physical properties has been a great challenge. In this work, a combination of surface pre-treatment and polymer nanocomposite coating is attempted for reducing degradation rate and improving biomineralization. The alloy surface was pickled in phosphoric acid and then coated with polydioxanone/hydroxyapatite nanocomposite. The samples were characterized using scanning electron microscopy (SEM) with energy dispersive spectroscopy (EDS) and x-ray diffraction (XRD). The corrosion resistance was studied using potentiodynamic polarization (PDP) test in 8.035 g/l NaCl solution. An immersion test in simulated body fluid (SBF) was also carried out to evaluate the biodegradation and biomineralization on the sample surfaces. Phosphoric acid pickling increased the corrosion resistance and adhesion between the coating and substrate. Polymer nanocomposite coating resulted in further control of degradation rate and enhanced biomineralization. Thus, pre-treated Mg-Ca alloys coated with polydioxanone/nHA composites can be considered as promising materials for developing degradable metallic implants.

**Keywords** biodegradation, coating, corrosion resistance, degradable implant, hydroxyapatite, in-vitro immersion, polydioxanone

## 1. Introduction

A temporary metallic orthopedic implant entails attributes like mechanical properties comparable to that of human bone, along with biocompatibility and biodegradability in physiological conditions (Ref 1). The conventional metallic implants can lead to complications such as stress shielding (Ref 2, 3), the release of

toxic metal ions (Ref 4), diagnostic image distortion (Ref 5), and a second surgery to remove them (Ref 1). The appropriate solution for this problem is to use biodegradable metallic materials that can degrade in the physiological environment at rates accordant with tissue growth. Magnesium (Mg) is one of the most suitable metals for biodegradable implant applications, as it is light in weight and exhibits mechanical properties compatible with that of human bone (Ref 6–8). Additionally, the degradation of Mg in the physiological environment will not produce any toxic by-products. Mg is also a necessary mineral and the excess Mg will be excreted through urine (Ref 9, 10). However, when compared with the pace of the bone tissue regeneration process, the degradation rate of Mg in the physiological environment is very high. In addition, the degradation process also leads to the release of hydrogen gas that can form subcutaneous gas cavities and obstruct bone-implant adhesion (Ref 11). Many techniques are reported by researchers to overcome the above issues, which include metallurgical and surface modifications of Mg-based alloys and composites (Ref 12–15). Metallurgical modifications were mainly achieved through alloying or composite fabrication (Ref 16–18), severe plastic deformation (SPD) methods (Ref 19, 20), and thermomechanical processing (TMP) (Ref 21, 22). Major alloying elements that are explored include, Ca, Zn, Zr, Sr, etc., and each of these elements has its own significance in deciding the biodegradation and mechanical behavior in the physiological environment (Ref 23, 24). Unlike other elements, the allowable daily usage of Ca in the human body is much higher and the same can be effectively used for tailoring the degradation of Mg. Mg-Ca alloys with enhanced corrosion resistance and mechanical properties can be advantageous for biodegradable

This invited article is part of a special topical focus in the *Journal of Materials Engineering and Performance* on Magnesium. The issue was organized by Prof. C. (Ravi) Ravindran, Dr. Raja Roy, Mr. Payam Emadi, and Mr. Bernoulli Andilab, Ryerson University.

**Mathew Gaius Cherian, Shebeer A. Rahim, and M.A. Joseph**, Department of Mechanical Engineering, National Institute of Technology Calicut, Kozhikode, Kerala, India; **V.P. Muhammad Rabeeh**, Nanomaterials Research Laboratory, School of Materials Science and Engineering, National Institute of Technology Calicut, Kozhikode, Kerala, India; and **T. Hanas**, Department of Mechanical Engineering, National Institute of Technology Calicut, Kozhikode, Kerala, India; and Nanomaterials Research Laboratory, School of Materials Science and Engineering, National Institute of Technology Calicut, Kozhikode, Kerala, India. Contact e-mail: hanas@nitc.ac.in.

implants (Ref 24). However, the addition of Ca beyond 1 wt.% decreases the corrosion resistance due to the precipitation of the Mg<sub>2</sub>Ca intermetallic phase along the grain boundaries (Ref 25). Hence, in this work, Mg-Ca alloys with 0.5 wt.% Ca are used as the base material.

Various surface modification methods are also proposed to control the biodegradation of Mg-based alloys (Ref 26, 27). The experimental and modeling studies on the degradation behavior of Mg also show promising results due to surface modification (Ref 28-30). Surface characteristics play a critical role in defining the corrosion resistance and biocompatibility of Mg-based alloys (Ref 31). Conversion coatings and deposited coatings are the prominent surface modification methods applied on Mg. Conversion coatings can serve as an adhesive layer for deposition coatings and subsequently result in a synergistic effect on degradation resistance and bioactivity (Ref 32-34). Conversion coatings developed by acid pickling of Mg alloys exhibited enhanced biomineralization due to the oxide layer formation (Ref 35). It also benefits removing surface impurities and increasing surface energy to improve the secondary coating adhesion. Such conversion coatings can be effectively used to improve the adhesion between the substrate and deposition coatings. Biodegradable polymers such as PCL, PVA, and PLA were explored as deposition coating on Mg for tailoring the degradation and biomineralization behavior in the physiological environment. Polydioxanone (PDS) is also a biodegradable and biocompatible polymer widely utilized in clinical applications as a suture material. The hydrophilic nature of PDS gives well adherence to the substrate surface and promotes cell adhesion (Ref 36-38).

Moreover, dispersion of hydroxyapatite (HA) in the polymer can promote apatite formation, as suggested by the reported works (Ref 39-42). A combination of acid treatment and PDS/HA composite coating on Mg-Ca alloy is not yet reported, and the same is explored in this work. The influence of acid pickling, the synergistic effect of pre-treatment and polymer-composite coating on the electrochemical corrosion, biodegradation and biomineralization in the physiological environment is clearly brought out in this work by conducting immersion studies in SBF.

## 2. Materials and Methods

### 2.1 Sample Preparation

The materials used include Mg-Ca alloy with 0.5% Ca (MatRICS, Kanyakumari, India), PDS (Sigma-Aldrich, India), nHA synthesized as reported by Rameshbabu et al. (Ref 43), and all other reagents of laboratory grade. The samples were cut to required dimensions and then polished using emery papers of grade up to 1500, followed by annealing at 350 °C for 1.5 h. The annealed samples were finely polished with 1-micron diamond paste, followed by cleaning with ethanol and drying. The samples were pre-treated using 1 M ortho-phosphoric acid (Fisher Scientific, assay = 88%) for 60 s at room temperature since wettability and corrosion resistance was better for this configuration (Ref 35).

### 2.2 Spin Coating of Mg-Ca Samples

The respective coating solutions were prepared in 1,1,1,3,3,3-hexafluoro-2-propanol (HFIP, SRL, India) as per the compositions mentioned in Table 1. For polymer-composite

samples, nHA was mixed with HFIP before being introduced to the polymer matrix for better dispersion (Ref 44). The solutions were magnetically stirred for 4 h at 600 rpm to distribute nHA uniformly without sedimentation. All the coated samples were acid pickled/pre-treated as mentioned in section 2.1 prior to coating. Samples were spin-coated (Spin150, APT, Germany) at 1000 rpm for 30 s to get stable films. On each sample, two coats were applied, and adequate drying time was assured before applying the final coat. The thickness of the developed samples was also recorded. The samples were termed B, AT, P, PC1, and PC2, and the features are summarized in Table 1.

### 2.3 Sample Surface Characterization

The synthesized nHA was characterized using SEM (Jeol 6390LA, USA) and XRD (X'Pert<sup>3</sup> MRD, PANalytical). The coating films were characterized using XRD with Cu K $\alpha$  radiation ( $\lambda=1.54 \text{ \AA}$ ) from 20 to 55° at a scanning rate of 1 step/s and step size of 0.002 °/step. The surface morphology and composition of bare Mg-Ca and coated samples were carried out by SEM with EDS (Oxford XMN, Oxford Instruments). The water contact angle was measured at multiple points using a surface measuring device (DMs-401, Kyowa Interface Science, Japan) to evaluate the variation in wettability. The tape removal method, as per ASTM D3359-17, determined the adhesive strength of coating onto the acid-treated surface. Additional samples of P and PC of dimension 4 × 4 × 0.3 cm were prepared to test the adhesion by method B-Cross-cut tape test using Elcometer 107 cross hatch cutter.

### 2.4 Electrochemical Test

All samples of dimension 2 × 2 × 0.3 cm were subjected to electrochemical impedance spectroscopy (EIS) and potentiodynamic polarization (PDP) test using an electrochemical workstation (Metrohm Autolab PGSTAT128N, Netherlands). The workstation consists of a three-electrode cell with the working electrode as the sample with an exposed area of 1 cm<sup>2</sup> to the electrolyte, Ag/AgCl<sub>3</sub> as the reference electrode and graphite rod as the counter electrode. The electrolyte used was a biomimetic NaCl solution with a concentration of 8.035 g/l since Cl ions induce pitting corrosion on Mg (Ref 45). The scanning rate was 1 mV/s, and the corrosion rates were calculated using a Tafel plot. EIS was measured from frequencies 10<sup>5</sup> to 10<sup>-1</sup> Hz. The sample with the lowest corrosion rate and maximum impedance among the PC variants was chosen for immersion studies along with B, AT, and P samples.

### 2.5 In-vitro Studies

A sufficient number of B, AT, P, and PC2 samples of dimension 1 × 1 × 0.3 cm were prepared for immersion studies. The immersion medium was conducted in simulated body fluid (SBF) which was prepared as mentioned by Kokubo et al. (Ref 46). Each sample was weighed and then immersed in an appropriate volume of SBF. The samples immersed in SBF were kept at a constant temperature of 37±1 °C in the water bath. Biodegradation, biomineralization, and pH variation studies were carried out for different periods of immersion, i.e., 1, 3, 7, 14, and 28 days. Samples were dried and weighed after respective periods of immersion to evaluate weight gain/loss. SEM-EDS characterization was used to study the morphology of immersed samples. The samples were then cleaned using boiling chromic acid (180 g/l) to remove the

depositions, polymer coating, and corrosion products. The final weight after the cleaning was also measured to calculate the corrosion rate using Eq 1, as per ASTM G31-72.

$$CR = \frac{(8.76 \times 10^4)W}{ATD} \quad (\text{Eq 1})$$

**Table 1** Compositional details of different samples

Sample	Acid Pickled, Y/N	PDS, w/v %	nHA, w/v %	Coating thickness, $\mu\text{m}$
B	N	...	...	...
AT	Y	...	...	...
P	Y	2.5	0	44
PC1	Y	2.5	2.5	15
PC2	Y	5	2.5	79

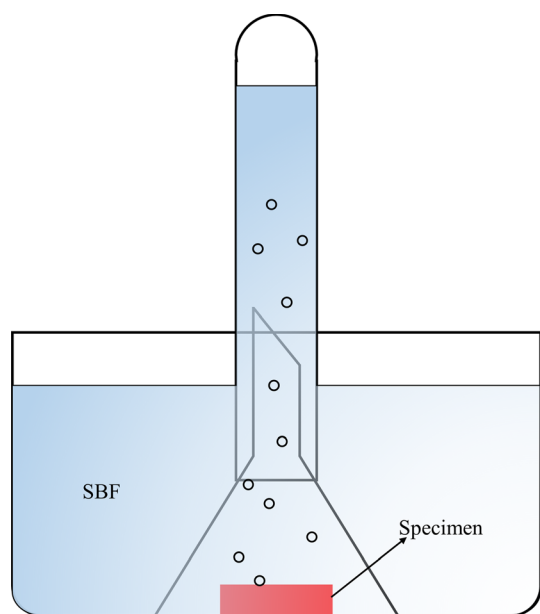


**Fig. 1** Schematic illustration of the H<sub>2</sub> measurement setup

CR is the corrosion rate in mm/year, W is the weight loss (g) that occurred in T hours of immersion, on an area of A cm<sup>2</sup> and D is the density of the sample, taken as 1.74 g/cm<sup>3</sup>. The rate of H<sub>2</sub> evolution was observed with a separate arrangement with an inverted test tube setup shown in Fig. 1 (Ref 47, 48). Since the volume that can be collected in a test tube is limited, the test could be conducted only for 5 days.

### 3. Results and Discussions

#### 3.1 Nano-Hydroxyapatite Characterization and Morphology

The XRD pattern of synthesized powder was in concurrence with that of the HA phase (JCPDS 09-432) and is shown in Fig. 2(a). Peak broadening was evident, indicating that the crystal size was near to the nanoscale regime, which was then validated by SEM analysis. The SEM images of powdered HA are shown in Fig. 2(b), and the majority of HA crystals were rod-shaped with a diameter of 18-24 nm and length 60-100 nm, approximately. The morphology also shows great affinity to

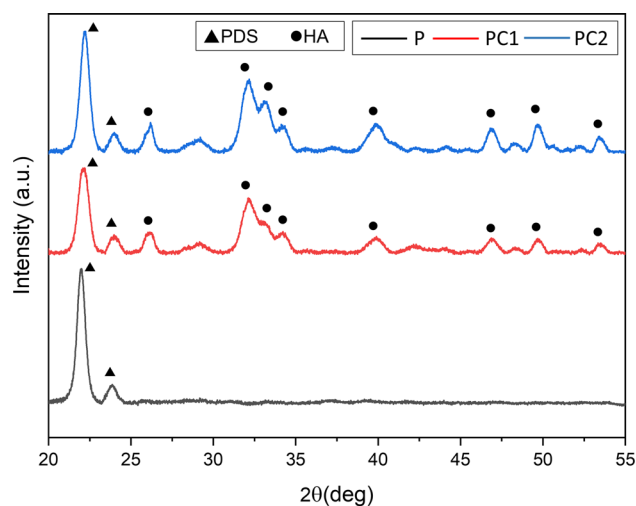


**Fig. 3** XRD pattern of different coating films

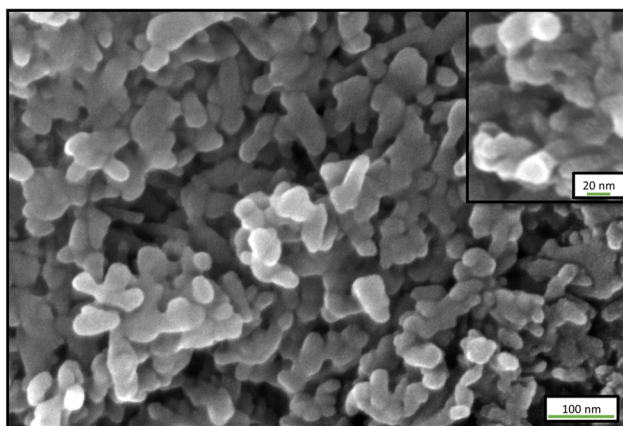
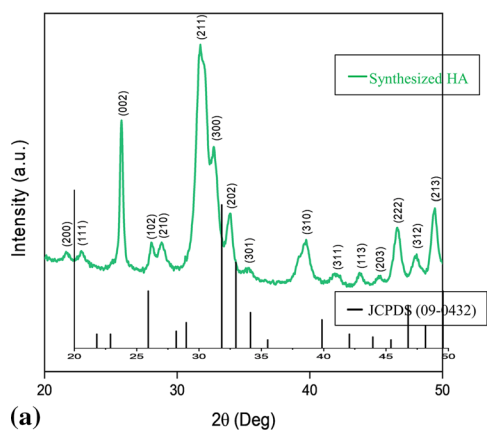


**Fig. 2** (a) XRD pattern and (b) SEM image of synthesized HA

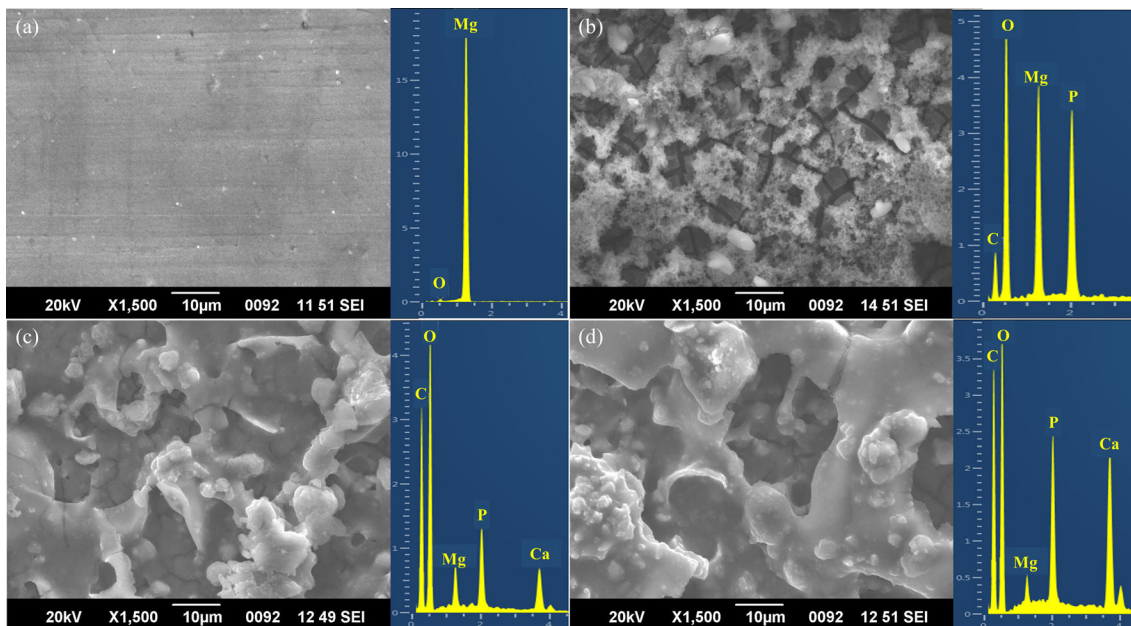


**Fig. 4** SEM-EDS analysis of (a) B, (b) P, (c) PC1 and (d) PC2 samples

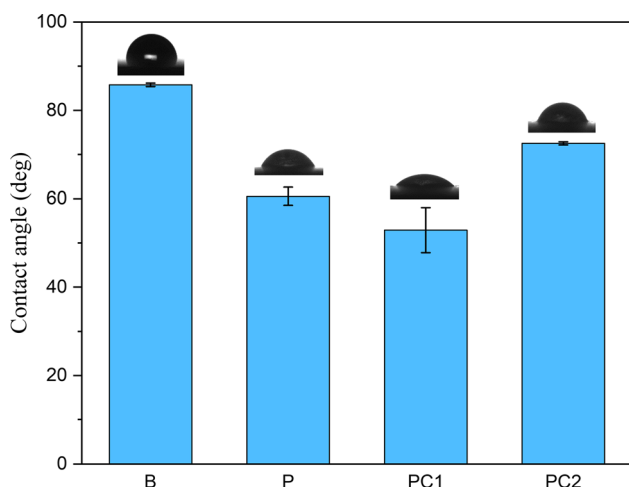


**Fig. 5** Water contact angle measurement on different samples

**Table 2** Adhesion grade as per ASTM D3359-17 of coated samples

Sample	No. of Grids Removed	ASTM Grade
P	0	5B
PC1	0	5B
PC2	0	5B

agglomerate due to the effect of oven drying during synthesis (Ref 43).

### 3.2 Characterization of Coated Samples

The diffraction peaks of PDS and nHA are identified in the XRD pattern of different coating films shown in Fig. 3. The peaks at 21.95 and 23.87° belong to PDS and the rest to nHA,

indicating successful development of the PDS-nHA composite. The surface morphology and composition for B, P, and PC samples using SEM-EDS are shown in Fig. 4. The Mg, P, and O peaks of P and PC samples indicate the formation of magnesium phosphate ( $Mg_3(PO_4)_2$ ) during acid-pickling (Ref 35). Unlike the polymer coating, the composite coatings have crack-free morphology. Figure 5 shows the contact angle measurements of B, P and PC samples, which computes the wettability of the sample surface. Hydrophilic surfaces can considerably enhance cell attachment and proliferation in a biological environment (Ref 49). A 29.4% reduction in contact angle was observed in P due to the combined effect of acid pickling and PDS coating. For PC1, the addition of nHA to PDS further reduced contact angle since nHA enhances surface roughness (Ref 39). However, the readings for PC2 samples recorded a slight increase, which could be due to the smooth coating surface developed due to higher PDS w/v% in PC2 samples, which is evident by SEM images. The contact angle for acid-treated samples was too low to compare, indicating the highly hydrophilic nature of the surface (Ref 35). Extremely high wettability is undesirable in biodegradable applications because it inhibits critical cellular interactions (Ref 50).

According to the ASTM D3359-17 standard mentioned in section 2.3, the coating adhesion grading of P and PC samples was measured and listed in Table 2. The number of grids from which the coating was partially or completely removed during the test was mapped with ASTM standard adhesion grade. ASTM grade 5B corresponds that none of the lattice squares formed by cross-hatching detached on tape removal. The deposited coatings have strong adherence because of the increased surface energy due to the acid pickling. Improved corrosion protection performance is expected due to good adhesion between coating and substrate.

### 3.3 Electrochemical Test

The Tafel plot for all samples is shown in Fig. 6(a), and electrochemical parameters are compiled in Table 3. The

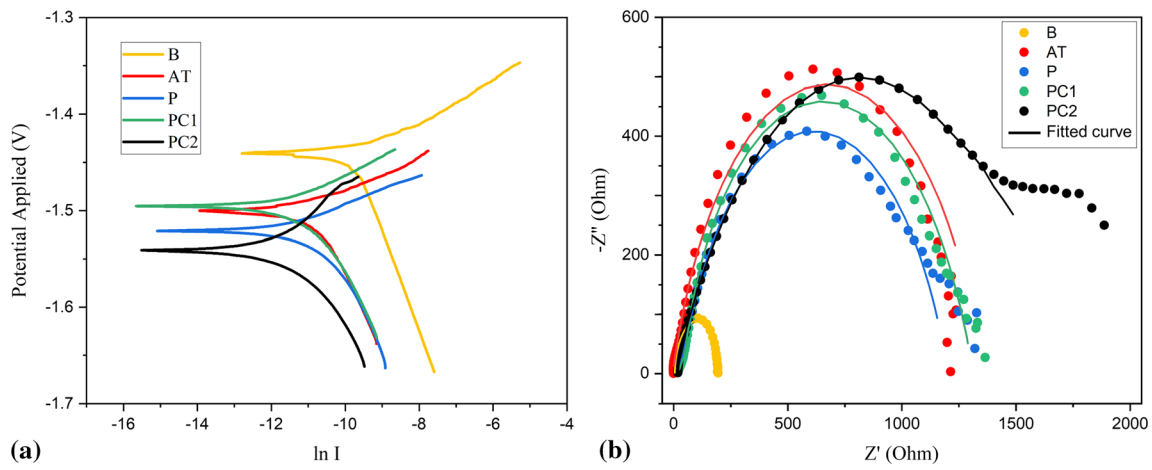


Fig. 6 Tafel plot and Nyquist plot for different variants

Table 3 Electrochemical parameters of different samples

Potentiodynamic polarization test				Electrochemical Impedance Spectroscopy				
Sample	$E_{\text{corr}}$ , V	$I_{\text{corr}}$ , $\mu\text{A}/\text{cm}^2$	CR, mm/year	$R_s$ , $\Omega$	$R_{\text{cp}}$ , $\Omega$	$Q_{\text{cp}}$ , $\text{F.s}^{(n-1)}$	$Q_{\text{dl}}$ , $\text{F.s}^{(n-1)}$	$R_{\text{ct}}$ , $\Omega$
Bare	-1.444	55.752	1.2792	3.738	...	...	$66.6 \times 10^{-6}$	196.2
AT	-1.503	28.064	0.5066	24.345	126.678	$33.5 \times 10^{-6}$	$0.9 \times 10^{-3}$	606.4
P	-1.507	17.022	0.3905	20.86	36.36	$3.5 \times 10^{-6}$	$45.4 \times 10^{-6}$	1089
PC1	-1.487	13.770	0.3160	20.72	92.45	$37.3 \times 10^{-6}$	$44.7 \times 10^{-6}$	1116
PC2	-1.541	7.545	0.1731	32.23	226.4	$58.9 \times 10^{-6}$	$7.02 \times 10^{-6}$	1384

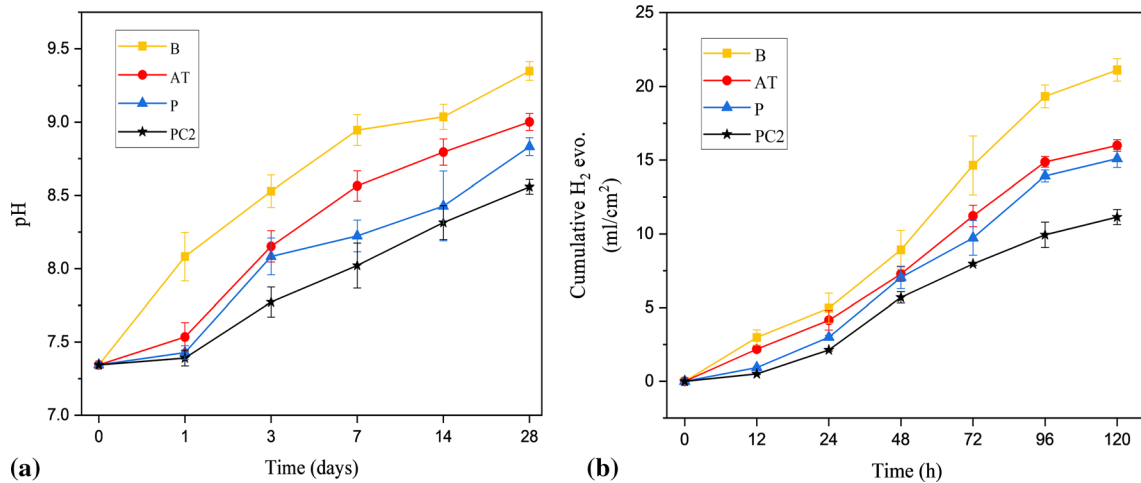


Fig. 7 pH variation and H<sub>2</sub> evolution recorded for different samples

corrosion current density ( $I_{\text{corr}}$ ) for bare Mg-Ca alloy was measured as  $55.752 \mu\text{A}/\text{cm}^2$ . The lowest value of  $I_{\text{corr}}$  measured was  $7.545 \mu\text{A}/\text{cm}^2$  for the PC2 variant, explaining the notable decrease in corrosion rate. A significant decrease of 60.4 % in corrosion rate was observed for AT compared to bare Mg-Ca due to magnesium phosphate layer formation. Deposition coating on treated samples further diminished the corrosion rate up to 86.5% in the PC2 sample indicating a reduction as

the PDS content increases. The same trend was observed in EIS studies and the Nyquist plot along with fitted curves and equivalent circuits are depicted in Fig. 6(b). From the fitted EIS parameters (Table. 3), the  $R_{\text{ct}}$  value of PC2 was found to be 1384  $\Omega$ , which is maximum among all samples and indicates that the enhancement in corrosion resistance occurs after composite coating.

### 3.4 Immersion Studies in SBF

**3.4.1 pH Variation.** Figure 7(a) depicts the pH variations during the immersion test of different samples. All samples exhibited an increasing trend in pH value over the 28-days study period. This increase is due to the formation of alkaline magnesium hydroxide as a degradation product on the substrate. When compared to bare Mg-Ca, the coated and acid-treated samples invariably had lower pH values. After 28 days of testing, the bare Mg-Ca sample had a maximum pH value of

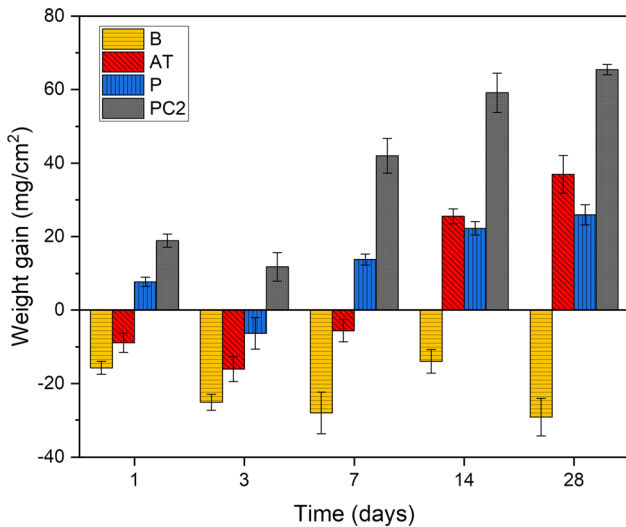


**Fig. 8** Weight gain/loss measured during immersion study for different samples

9.3, and the PC2 variant had a minimum of 8.5. The acid-treated and polymer-coated samples had pH values 9 and 8.8 after 28 days, respectively. The pH drop in coated samples also correlates to the PDS proportion in the coating. It is worth noting that the pH variation in a real system will be lesser than these results as the system will be more dynamic, unlike the static immersion test performed.

**3.4.2 H<sub>2</sub> Gas Evolution.** Figure 7(b) presents the cumulative H<sub>2</sub> gas evolution from the samples during the immersion test in SBF. During the test period, the bare Mg-Ca samples developed the highest amount of H<sub>2</sub>, with the fastest release rate. The cumulative H<sub>2</sub> evolution of bare samples was reduced by acid treatment. The coated and pre-treated samples further reduced the evolution. Compared to the bare Mg-Ca sample, the PC2 sample reduced cumulative H<sub>2</sub> evolution by 39.7% after 120 h. Due to the combined influence of conversion and deposition coatings, the initial evolution rates of H<sub>2</sub> for the P and PC2 samples are significantly low. This indicates that the treatment and coating can help in keeping the surface stable during the initial period of immersion.

**3.4.3 Weight Gain and Biomineralization.** After the immersion test, the samples were dried and weight gain/loss was measured immediately. The variation in weight for all samples is shown in Fig. 8. AT displayed weight loss during the initial period followed by gain after 14 days. The gain in weight could be due to the presence of conversion coating that promoted biomineralization (Ref 35, 51). After three days, the weight loss in P might be related to the degradation of the PDS protective coating. However, the sample started recording a weight gain later, indicating deposition of biomineralization products. The phosphate layer formed during acid pickling and the PDS deposited synergistically helped in providing a

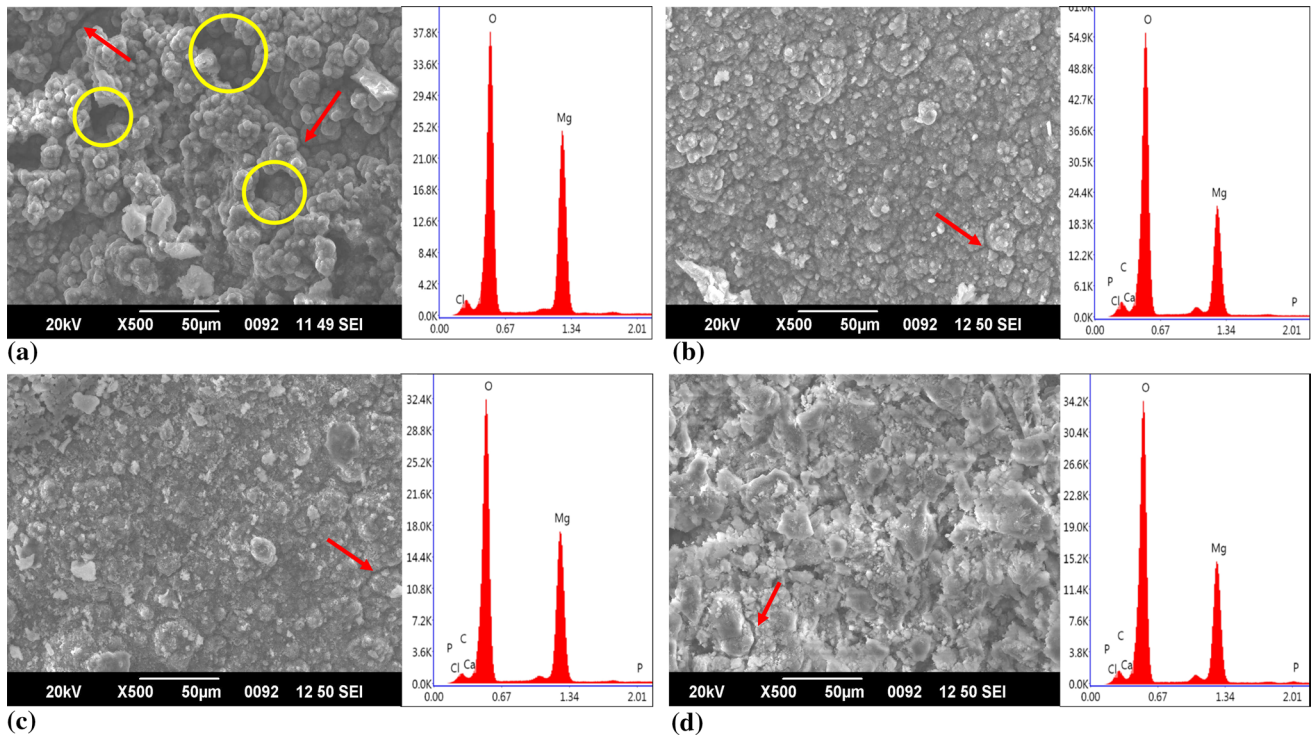


**Fig. 9** SEM-EDS analysis of (a) B, (b) P, (c) PC1 and (d) PC2 immersion samples. (Yellow circles indicate pitting corrosion and the red arrows point toward the cracks.)

stable platform for nucleation and growth of CaP on the coated surfaces. The influence of bioactive nHA further helped in the process and hence the composite coated PC2 samples recorded higher weight gain over other samples.

The quantitative and qualitative analysis of biomineralization could not be performed as the deposition products did not adhere to the surface of the samples for further handling. The samples thus obtained were then analyzed using microscopy and EDS after the immersion test, without the depositions on the sample. Figure 9 depicts the morphology and EDS analysis of the samples. Pitting corrosion and cracks can be observed throughout the bare Mg-Ca sample. Pitting corrosion resistance improved for acid-treated samples due to  $Mg_3(PO_4)_2$  conversion layer; however, minor cracks are apparent. Nucleation and growth can be found on the surface of AT and PC samples. Morphology of the treated and coated samples shows a significant difference from that of bare samples. While the depositions on the bare samples are irregular in shape and size, the same on the coated and treated samples show distinct morphologies. Such morphologies are seen when the surfaces help in the formation of crystals through nucleation and growth (Ref 51, 52). An irregular or large polygonal depositions are usually observed when there is no protection to avoid precipitation due to a change in local pH.

**3.4.4 Degradation Rate.** The corrosion rates calculated from the weight loss after immersion test are summarized in Fig. 10. It is observed that the composite coated samples exhibited a 60% reduction in the degradation rate during the initial period of the immersion test. This reduction is attributed to the synergistic performance of the layers developed by acid treatment and spin coating. While the polymer composite coating protected the surface beneath, the conversion coating helped in improving the adhesion at the interface. Both the layers supported each other, and thus the surface became conducive for biomineralization. The CaP thus developed on the sample surface helped in further reducing the degradation rate. Although the AT sample corroded faster than P over the first 14 days, the rates were almost identical after 28 days. This may be due to the degradation of the polymeric layer toward the

end of the immersion test. As exhibited by the PC2 samples, the presence of HA can not only reinforce the polymer but also enhance the biomineralization on the surface. Such layer formed on the surface can easily protect the substrate beneath and promote further biomineralization as well as reduce degradation rate.

## 4. Conclusions

A PDS-HA nanocomposite coating was developed by spin coating on phosphoric acid-pickled Mg-Ca alloy. The reduction in degradation rate was analyzed using the electrochemical corrosion test and immersion test in SBF. Significant reduction in corrosion rate,  $H_2$  evolution and pH variation was confirmed due to the synergistic effect of PDS/nHA coating and the conversion layer formed by acid-pickling. When compared to bare Mg-Ca, the initial corrosion rate and  $H_2$  evolution of the PC2 sample were reduced by 59.14 and 83.17 %, respectively. The pH value increased by 27.29 % in the B sample, but only 16.53 % in the PC2 type. Hence, it is concluded that PDS/nHA composite coating combined with acid pickling can serve as an effective surface coating method to tailor the degradation rate of Mg-Ca alloy in the physiological environment.

## Acknowledgment

The authors gratefully acknowledge the financial grant No. 5/4-5/3ORTHO/2019-NCD-I Dt.16-09-2019 from the Indian Council of Medical Research (ICMR) and Centre for Materials Characterization, NIT Calicut for providing the XRD facility.

## References

1. C. Li, C. Guo, V. Fitzpatrick, A. Ibrahim, M.J. Zwierstra, P. Hanna, A. Lechtig, A. Nazarian, S.J. Lin and D.L. Kaplan, Design of Biodegradable, Implantable Devices towards Clinical Translation, *Nat. Rev. Mater.*, 2020, **5**(1), p 61-81. <https://doi.org/10.1038/s41578-019-0150-z>
2. H.S. Han, S. Loffredo, I. Jun, J. Edwards, Y.C. Kim, H.K. Seok, F. Witte, D. Mantovani and S. Glyn-Jones, Current Status and Outlook on the Clinical Translation of Biodegradable Metals, *Mater. Today*, 2019, **23**, p 57-71. <https://doi.org/10.1016/j.mattod.2018.05.018>
3. J. Jiao, S. Zhang, X. Qu and B. Yue, Recent Advances in Research on Antibacterial Metals and Alloys as Implant Materials, *Front. Cell. Infect. Microbiol.*, 2021 <https://doi.org/10.3389/fcimb.2021.693939>
4. Z. Li and K.A. Khor, Preparation and Properties of Coatings and Thin Films on Metal Implants, *Encyclopedia of Biomedical Engineering*. Elsevier, 2019
5. M. Cassetta, N. Pranno, A. Stasolla, N. Orsogna, D. Fierro, C. Cavallini and V. Cantisani, The Effects of a Common Stainless Steel Orthodontic Bracket on the Diagnostic Quality of Cranial and Cervical 3T- MR Images: A Prospective Case-Control Study, *Dentomaxillofacial Radiol.*, 2017, **46**(6), p 1-13
6. W. Li, W. Qiao, X. Liu, D. Bian, D. Shen, Y. Zheng, J. Wu, K.Y.H. Kwan, T.M. Wong, K.M.C. Cheung and K.W.K. Yeung, Biomimicking Bone-Implant Interface Facilitates the Bioadaptation of a New Degradable Magnesium Alloy to the Bone Tissue Microenvironment, *Adv. Sci.*, 2021, **8**(23), p 1-17
7. J.L. Wang, J.K. Xu, C. Hopkins, D.H.K. Chow and L. Qin, Biodegradable Magnesium-Based Implants in Orthopedics—A General Review and Perspectives, *Adv. Sci.*, 2020, **7**(8), p 1902443
8. M. Chagnon, L.G. Guy and N. Jackson, Evaluation of Magnesium-Based Medical Devices in Preclinical Studies: Challenges and Points to Consider, *Toxicol. Pathol.*, 2019, **47**(3), p 390-400

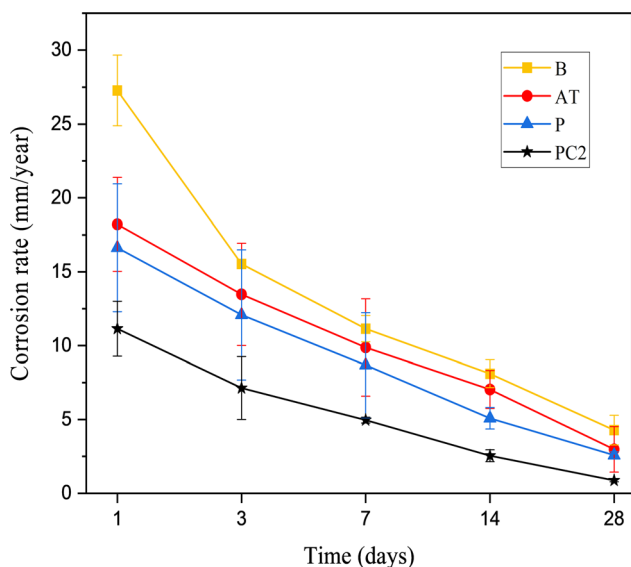


**Fig. 10** Corrosion rates were measured for different samples during the immersion period

9. N.L. Saris, E. Mervaala, H. Karppanen, J.A. Khawaja and A. Lewenstam, Magnesium An Update on Physiological, Clinical and Analytical Aspects, *Clin. Chim. acta*, 2000, **294**(1-2), p 1-26
10. L. Xu, R. Willumeit-Römer and B.J.C. Luthringer-Feyerabend, Effect of Magnesium-Degradation Products and Hypoxia on the Angiogenesis of Human Umbilical Vein Endothelial Cells, *Acta Biomater.*, 2019, **98**, p 269-283
11. D. Persaud-Sharma and A. McGoron, Biodegradable Magnesium Alloys: A Review of Material Development and Applications, *J. Biomim. Biomater. Tissue Eng.*, 2012, **12**(1), p 25-39
12. S. Prasad, V. Ratheesh, V. Manakari, G. Parande, M. Gupta and R. Wong, The Potential of Magnesium Based Materials in Mandibular Reconstruction, *Metals (Basel)*, 2019, **9**(3), p 1-20
13. S.A. Rahim, M.A. Joseph, T.S.S. Kumar and T. Hanas, Recent Progress in Surface Modification of Mg Alloys for Biodegradable Orthopedic Applications, *Front. Mater.*, 2022, **9**(848980), p 1-21. <https://doi.org/10.3389/fmats.2022.848980>
14. S. Prasad, G. Parande, M. Gupta and R. Wong, Compositional Tailoring of Mg-2Zn-1Ca Alloy Using Manganese to Enhance Compression Response and In-Vitro Degradation, *Materials (Basel)*, 2022, **15**(3), p 810
15. V. Tsakiris, C. Tardei and F.M. Clicinschi, Biodegradable Mg Alloys for Orthopedic Implants - A Review, *J. Magnes. Alloy.*, 2021, **9**(6), p 1884-1905
16. L. Hong, R. Wang and X. Zhang, The Role of Nd in Corrosion Properties of Mg-12Gd-2Zn-0.4Zr Alloys, *J. Mater. Eng. Perform.*, 2021, **30**(8), p 6000-6008
17. T.O. Olugbade, B.O. Omiyale and O.T. Ojo, Corrosion, Corrosion Fatigue, and Protection of Magnesium Alloys: Mechanisms, Measurements, and Mitigation, *J. Mater. Eng. Perform.*, 2021, **31**(3), p 1707-1727
18. M.S. Kujur, V. Manakari, G. Parande, S. Prasad, R. Wong, A. Mallick and M. Gupta, Development of Rare-Earth Oxide Reinforced Magnesium Nanocomposites for Orthopaedic Applications: A Mechanical/Immersion/Biocompatibility Perspective, *J. Mech. Behav. Biomed. Mater.*, 2021, **114**, p 104162
19. C.L.P. Silva, A.C. Oliveira, C.G.F. Costa, R.B. Figueiredo, M. de Fátima, M.M. Leite, V.F.C. Pereira, T.G. Lins and Langdon, Effect of Severe Plastic Deformation on the Biocompatibility and Corrosion Rate of Pure Magnesium, *Journal of Materials Science*, 2017, **52**(10), p 5992-6003
20. B. Chen, C. Xin, G. Zhang, F. Zhou and L. Zhang, Grain-Refined Microstructure and Hard Surface Layer Produced by SMRGT Process for Improved Corrosion Behavior of Mg-3Al-1Zn Alloy, *J. Mater. Eng. Perform.*, 2019, **28**(2), p 1253-1262
21. H.B. Henderson, V. Ramaswamy, A.E. Wilson-Heid, M.S. Kesler, J.B. Allen and M.V. Manuel, Mechanical and Degradation Property Improvement in a Biocompatible Mg-Ca-Sr Alloy by Thermomechanical Processing, *J. Mech. Behav. Biomed. Mater.*, 2018, **80**, p 285-292. <https://doi.org/10.1016/j.jmbbm.2018.02.001>
22. N. Sriraman and S. Kumaran, Improved Bio-Acceptability of Thermomechanically Processed ZM21 Magnesium Alloy, *Mater. Res. Express*, 2019, **6**(5), p 056524
23. H. Li, Y. Zheng and L. Qin, Progress of Biodegradable Metals, *Prog. Nat. Sci. Mater. Int.*, 2014, **24**(5), p 414-422. <https://doi.org/10.1016/j.pnsc.2014.08.014>
24. Y. Ding, C. Wen, P. Hodgson and Y. Li, Effects of Alloying Elements on the Corrosion Behavior and Biocompatibility of Biodegradable Magnesium Alloys: A Review, *J. Mater. Chem. B*, 2014, **2**(14), p 1912-1933
25. Z. Li, X. Gu, S. Lou and Y. Zheng, The Development of Binary Mg-Ca Alloys for Use as Biodegradable Materials within Bone, *Biomaterials*, 2008, **29**(10), p 1329-1344
26. Y. Gu, X. Zheng, Q. Liu, H. Ma, L. Zhang and D. Yang, Investigating Corrosion Performance and Corrosive Wear Behavior of Sol-Gel/MAO-Coated Mg Alloy, *Tribol. Lett.*, 2018, **66**(3), p 1-15
27. X. Zheng, Q. Liu, H. Ma, S. Das, Y. Gu and L. Zhang, Probing Local Corrosion Performance of Sol-Gel/MAO Composite Coating on Mg Alloy, *Surf. Coatings Technol.*, 2018, **347**, p 286-296. <https://doi.org/10.1016/j.surfcoat.2018.05.010>
28. Z. Shen, M. Zhao, D. Bian, D. Shen, X. Zhou, J. Liu, Y. Liu, H. Guo and Y. Zheng, Predicting the Degradation Behavior of Magnesium Alloys with a Diffusion-Based Theoretical Model and in Vitro Corrosion Testing, *J. Mater. Sci. Technol.*, 2019, **35**(7), p 1393-1402. <https://doi.org/10.1016/j.jmst.2019.02.004>
29. M. Abdalla and H. Ibrahim, A Physical Approach to Simulate the Corrosion of Ceramic-coated Magnesium Implants, *Appl. Sci.*, 2021, **11**(15), p 6724
30. H. Ma, Y. Gu, S. Liu, J. Che and D. Yang, Local Corrosion Behavior and Model of Micro-Arc Oxidation HA Coating on AZ31 Magnesium Alloy, *Surf. Coatings Technol.*, 2017, **331**, p 179-188. <https://doi.org/10.1016/j.surfcoat.2017.10.053>
31. C. Pan, Y. Hu, Y. Hou, T. Liu, Y. Lin, W. Ye, Y. Hou and T. Gong, Corrosion Resistance and Biocompatibility of Magnesium Alloy Modified by Alkali Heating Treatment Followed by the Immobilization of Poly (Ethylene Glycol), Fibronectin and Heparin, *Mater. Sci. Eng. C*, 2017, **70**, p 438-449
32. D.B. Prabhu, P. Gopalakrishnan and K.R. Ravi, Morphological Studies on the Development of Chemical Conversion Coating on Surface of Mg-4Zn Alloy and Its Corrosion and Bio Mineralisation Behaviour in Simulated Body Fluid, *J. Alloys Compd.*, 2020, **812**, p 152146. <http://doi.org/10.1016/j.jallcom.2019.152146>
33. W. Zai, Y. Su, H.C. Man, J. Lian and G. Li, Effect of PH Value and Preparation Temperature on the Formation of Magnesium Phosphate Conversion Coatings on AZ31 Magnesium Alloy, *Appl. Surf. Sci.*, 2019, **492**, p 314-327. <https://doi.org/10.1016/j.apsusc.2019.05.309>
34. Y. Sasikumar, A. Madhan Kumar, R. Suresh Babu, P. Dhaviveegan, N. Al-Aqeeli and A.L.F. de Barros, Fabrication of Brushite Coating on AZ91D and AZ31 Alloys by Two-Step Chemical Treatment and Its Surface Protection in Simulated Body Fluid, *J. Mater. Eng. Perform.*, 2019, **28**(6), p 3803-3815. <https://doi.org/10.1007/s11665-019-04143-7>
35. S. Rahim, V.P. Muhammad Rabeeh, M.A. Joseph and T. Hanas, Does Acid Pickling of Mg-Ca Alloy Enhance Biomineralization?, *J. Magnes. Alloys*, 2021, **9**(3), p 1028-1038. <https://doi.org/10.1016/j.jma.2020.12.002>
36. A. Moshiri, A. Oryan and A. Meimandi-Parizi, Synthesis, Development, Characterization and Effectiveness of Bovine Pure Platelet Gel-Collagen-Polydioxanone Bioactive Graft on Tendon Healing, *J. Cell. Mol. Med.*, 2015, **19**(6), p 1308-1332
37. S. Saska, L. Pilatti, E. Santos, D.S. Silva, M.A. Nagasawa, C. Diana, B. Kempisty, S. Tunchel, N. Lizier, E. Finger and M. Dyszkiewicz, Polydioxanone-Based Membranes for Bone Regeneration, *Polymers*, 2021, **13**(11), p 1685
38. J.A. Martins, A.A. Lach, H.L. Morris, A.J. Carr and P. Mouthuy, Polydioxanone Implants: A Systematic Review on Safety and Performance in Patients, *J. Biomater. Appl.*, 2020, **34**(7), p 902-916
39. T. Hanas, T.S. Sampath Kumar, G. Perumal, M. Doble and S. Ramakrishna, Electrospun PCL/HA Coated Friction Stir Processed AZ31/HA Composites for Degradable Implant Applications, *J. Mater. Process. Technol.*, 2018, **252**, p 398-406
40. P. Bansal, G. Singh and H.S. Sidhu, Plasma-Sprayed Hydroxyapatite-Strontium Coating for Improved Corrosion Resistance and Surface Properties of Biodegradable AZ31 Mg Alloy for Biomedical Applications, *J. Mater. Eng. Perform.*, 2021, **30**, p 1768-1779. <https://doi.org/10.1007/s11665-021-05490-0>
41. A. Dubey, S. Jaiswal and D. Lahiri, Mechanical Integrity of Biodegradable Mg-HA Composite During In Vitro Exposure, *J. Mater. Eng. Perform.*, 2019, **28**(2), p 800-809. <https://doi.org/10.1007/s11665-018-3778-8>
42. G. Parande, V. Manakari, S. Prasad, D. Chauhan, S. Rahate, R. Wong and M. Gupta, Strength Retention, Corrosion Control and Biocompatibility of Mg-Zn-Si/HA Nanocomposites, *J. Mech. Behav. Biomed. Mater.*, 2020, **103**, 103584
43. N. Rameshbabu, K. Prasad Rao and T.S. Sampath Kumar, Accelerated Microwave Processing of Nanocrystalline Hydroxyapatite, *J. Mater. Sci.*, 2005, **40**(23), p 6319-6323. <https://doi.org/10.1007/s10853-005-2957-9>
44. I.A. Rodriguez, P.A. Madurantakam, J.M. McCool, S.A. Sell, H. Yang, P.C. Moon and G.L. Bowlin, Mineralization Potential of Electrospun PDO-Hydroxyapatite-Fibrinogen Blended Scaffolds, *Int. J. Biomater.*, 2012 <https://doi.org/10.1155/2012/159484>
45. M.P. Stager, A.M. Pietak, J. Huadmai and G. Dias, Magnesium and Its Alloys as Orthopedic Biomaterials: A Review, *Biomaterials*, 2006, **27**(9), p 1728-1734. <https://doi.org/10.1016/j.biomaterials.2005.10.003>
46. T. Kokubo and H. Takadama, How Useful Is SBF in Predicting in Vivo Bone Bioactivity?, *Biomaterials*, 2006, **27**, p 2907-2915



47. S. Swati Gaur, R.K. Singh Raman and A.S. Khanna, In Vitro Investigation of Biodegradable Polymeric Coating for Corrosion Resistance of Mg-6Zn-Ca Alloy in Simulated Body Fluid, *Mater. Sci. Eng.: C*, 2014, **42**, p 91-101. <https://doi.org/10.1016/j.msec.2014.05.035>
48. N.T. Kirkland, N. Birbilis and M.P. Staiger, Assessing the Corrosion of Biodegradable Magnesium Implants: A Critical Review of Current Methodologies and Their Limitations, *Acta Biomater.*, 2012, **8**(3), p 925-936. <https://doi.org/10.1016/j.actbio.2011.11.014>
49. W. Hong, F. Guo, J. Chen, X. Wang, X. Zhao and P. Xiao, Bioactive Glass-Chitosan Composite Coatings on PEEK: Effects of Surface Wettability and Roughness on the Interfacial Fracture Resistance and in Vitro Cell Response, *Appl. Surf. Sci.*, 2018, **440**, p 514-523. <https://doi.org/10.1016/j.apsusc.2018.01.183>
50. K.L. Menzies and L. Jones, The Impact of Contact Angle on the Biocompatibility of Biomaterials, *Optom. Vis. Sci.*, 2010, **87**(6), p 387-399
51. T. Hanas, T.S. Sampath Kumar, G. Perumal and M. Doble, Tailoring Degradation of AZ31 Alloy by Surface Pre-Treatment and Electrospun PCL Fibrous Coating, *Mater. Sci. Eng.: C*, 2016, **65**, p 43-50. <https://doi.org/10.1016/j.msec.2016.04.017>
52. A. Dubey, S. Jaiswal, S. Haldar, P. Roy and D. Lahiri, Mg-3Zn / HA Biodegradable Composites Synthesized via Spark Plasma Sintering for Temporary Orthopedic Implants, *J. Mater. Eng. Perform.*, 2019, **28**(9), p 5702-5715

**Publisher's Note** Springer Nature remains neutral with regard to jurisdictional claims in published maps and institutional affiliations.